New Journal of Physics
The open access journal at the forefront of physics

Deutsche Physikalische Gesellschaft DPG IOP Institute of Physics

PAPER • OPEN ACCESS

# Broadband frequency conversion of ultrashort pulses using high-*Q* metasurface resonators

To cite this article: Timo Stolt and Mikko J Huttunen 2022 *New J. Phys.* **24** 025004

View the article online for updates and enhancements.

You may also like

- Active optical metasurfaces: comprehensive review on physics, mechanisms, and prospective applications
Jingyi Yang, Sudip Gurung, Subhajit Bej et al.
- Metasurfaces: a new look at Maxwell's equations and new ways to control light
M A Remnev and V V Klimov
- Resonant dielectric metasurfaces: active tuning and nonlinear effects
Chengjun Zou, Jürgen Sautter, Frank Setzpfandt et al.

This content was downloaded from IP address 130.230.128.128 on 30/03/2022 at 10:15

New Journal of Physics
The open access journal at the forefront of physics

Deutsche Physikalische Gesellschaft DPG
IOP Institute of Physics

Published in partnership with: Deutsche Physikalische Gesellschaft and the Institute of Physics

OPEN ACCESS

RECEIVED
27 October 2021

REVISED
20 December 2021

ACCEPTED FOR PUBLICATION
11 January 2022

PUBLISHED
9 February 2022

Original content from this work may be used under the terms of the Creative Commons Attribution 4.0 licence.

Any further distribution of this work must maintain attribution to the author(s) and the title of the work, journal citation and DOI.

PAPER

# Broadband frequency conversion of ultrashort pulses using high-*Q* metasurface resonators

**Timo Stolt and Mikko J Huttunen***

Photonics Laboratory, Physics Unit, Tampere University, FI-33014 Tampere, Finland
* Author to whom any correspondence should be addressed.

**E-mail:** mikko.huttunen@tuni.fi

**Keywords:** nonlinear optics, metasurfaces, surface lattice resonance, plasmonics, frequency conversion

## Abstract

Frequency conversion of light can be dramatically enhanced using high quality factor (*Q*-factor) resonator. Unfortunately, the achievable conversion efficiencies and conversion bandwidths are fundamentally limited by the time–bandwidth limit of the resonator, restricting their use in frequency conversion of ultrashort pulses. Here, we propose and numerically demonstrate sum-frequency generation based frequency conversion using a metasurface-based resonator configuration that could overcome this limitation. The proposed experimental configuration takes use of the spatially dispersive responses of periodic metasurfaces supporting collective surface lattice resonances (SLRs), and can be utilized for broadband frequency conversion of ultrashort pulses. We investigate a plasmonic metasurface, supporting a high-*Q* SLR ($Q = 500$, linewidth of 2 nm) centered near 1000 nm, and demonstrate ∼1000-fold enhancements of nonlinear signals. Furthermore, we demonstrate broadband frequency conversion with a pump conversion bandwidth reaching 75 nm, a value that greatly surpasses the linewidth of the studied resonator. Our work opens new avenues to utilize high-*Q* metasurfaces for broadband nonlinear frequency conversion.

Since the construction of the first laser in 1960, lasers have been the most common instruments to generate intense, coherent, monochromatic, and directional light [1]. When applying specific techniques, such as *Q*-switching and mode-locking, lasers can be used to generate ultrashort pulses with extremely high peak intensities and pulse durations down to a few femtoseconds. A major drawback of ultrashort pulse lasers is the lack of tunability. Visible and infrared spectral regions are commonly accessed by utilizing nonlinear frequency conversion resulting from nonlinear processes, such as second-harmonic generation (SHG), sum-frequency generation (SFG), or difference-frequency generation (DFG) [2]. Unfortunately, nonlinear processes are, by their nature, extremely inefficient. Conventional nonlinear optical devices overcome this drawback by utilizing phase-matching techniques and optical resonators [2]. Even though these techniques solve the efficiency problem, their operation bandwidths are often quite narrow, restricting their use in frequency conversion of ultrashort pulses with broad spectral features. This trade-off between conversion efficiency and bandwidth can be solved using adiabatic frequency conversion [3, 4]. However, such techniques rely on long propagation lengths and complicated phase-matching schemes in the nonlinear medium, motivating to seek for alternative approaches.

Recent progress in the fabrication of nanostructures has enabled the development of a novel material class called metamaterials [5]. They are artificial structures consisting of nanoscale building blocks such as nanoparticles (NPs) and gratings. Interestingly, the optical properties of metamaterials can be engineered by tuning the properties of the building blocks, such as their size and shape, during the fabrication process. As a result, metamaterials can exhibit exotic properties, such as negative index of refraction, epsilon-near-zero behavior at optical frequencies, and nanoscale phase-engineering capabilities [6–9].

Plasmonic metasurfaces consisting of metallic NPs have recently shown the potential for enhancing nonlinear processes in nanoscale structures [10]. Metal NPs exhibit collective oscillations of the conduction

© 2022 The Author(s). Published by IOP Publishing Ltd on behalf of the Institute of Physics and Deutsche Physikalische Gesellschaft

electrons giving rise to localized surface plasmon resonances (LSPRs) [11], which result in an increased local field near the NP, subsequently enhancing the nonlinear response [12–18]. However, LSPRs are associated with low quality factors ($Q$-factors, $Q < 10$) due to the high ohmic losses associated with plasmon resonances. Fortunately, periodically arranged NPs exhibit surface lattice resonances (SLRs) [19, 20], that are associated with narrow spectral features and thus of much higher $Q$-factors ($Q \approx 2300$) than LSPRs [21]. Therefore, SLRs can result in dramatic local-field enhancements and consequent enhancement of nonlinear responses [22–24].

Despite the potential of utilizing SLR-based metasurface resonators for frequency conversion, their behavior is restricted by the time–bandwidth limit associated with optical resonators [25]. Further enhancement of the local fields present near the NPs by designing SLRs with $Q$-factors will simultaneously limit their use to frequency conversion of spectrally broad laser sources [21]. Therefore, use of high-$Q$ metasurfaces is seemingly restricted to spectrally narrow laser sources and subsequent nonlinear applications.

In this work, we propose an experimental configuration to achieve broadband frequency conversion with a single plasmonic metasurface supporting a high-$Q$ SLR resonator ($Q \approx 500$, center wavelength 1002 nm, linewidth of 2 nm). The proposed setup utilizes a temporal-focusing scheme that first separates an incident broadband laser beam into separate spectral components that interact nonlinearly with the metasurface. The spatial dispersion of SLRs allows us to couple these different spectral components of the incident beam, arriving at the metasurface at different incidence angles, optimally with the SLR of the metasurface. After the nonlinear interaction, the generated signal frequency components are then combined to form the broadband output beam. Effectively, the use of the proposed scheme results in a broadband enhancement of SHG and SFG processes. We numerically show resonance-enhanced SFG exhibiting a pump conversion bandwidth of $\Delta\lambda \approx 75$ nm (1020–1095 nm), a value greatly exceeding the 2 nm linewidth of the SLR.

## 1. Theory

The nonlinear response of a metasurface can be evaluated using nonlinear scattering theory [26, 27]. Using this approach, the SFG response of a metasurface depends on the mode overlap between local fields at the fundamental frequencies $\mathbf{E}(\omega_1, \mathbf{r})$ and $\mathbf{E}(\omega_2, \mathbf{r})$, and at the SFG frequency $\mathbf{E}(\omega_3, \mathbf{r})$ [28–30]. Consequently, the detected far-field SFG emission $\mathbf{E}_{\text{det}}$ $(\omega_3 = \omega_1 + \omega_2)$ can be estimated using the Lorentz reciprocity theorem as [26]

$$\mathbf{E}_{\text{det}}(\omega_3 = \omega_1 + \omega_2) \propto \iiint_V \chi^{(2)}(\omega_3; \omega_1, \omega_2, \mathbf{r}) : \mathbf{E}(\omega_1, \mathbf{r})\mathbf{E}(\omega_2, \mathbf{r})\mathbf{E}^*(\omega_3, \mathbf{r})\, \mathrm{d}V, \tag{1}$$

where integration is performed over metasurface unit cell volume $V$, and $\chi^{(2)}(\omega_3;\ \omega_1, \omega_2, \mathbf{r})$ is the nonlinear susceptibility tensor. For SHG, where $\omega_1 = \omega_2 = \omega$ and $\omega_3 = 2\omega$, equation (1) is written as

$$\mathbf{E}_{\text{det}}(2\omega) \propto \iiint_V \chi^{(2)}(2\omega; \omega, \omega, \mathbf{r}) : \mathbf{E}^2(\omega, \mathbf{r})\mathbf{E}^*(2\omega, \mathbf{r})\, \mathrm{d}V. \tag{2}$$

The local fields $\mathbf{E}(\omega_i, \mathbf{r})$ consist of the incident laser field $\mathbf{E}_{\text{inc}}(\mathbf{k}_i, \omega_i)$, where $\mathbf{k}_i$ is the laser field wave vector, and of the field scattered by the nanoparticles in the metasurface $\mathbf{E}_{\text{scat}}(\omega_i)$. In other words, $\mathbf{E}(\omega_i) = \mathbf{E}_{\text{inc}}(\mathbf{k}_i, \omega_i) + \mathbf{E}_{\text{scat}}(\omega_i)$. Consequently, the local fields can be increased either by increasing the incident laser field amplitude, or by utilizing resonances, such as LSPRs or SLRs, that boost the scattered fields $\mathbf{E}_{\text{scat}}(\omega_i)$ [31].

In this work, we focus on SLRs that occur in periodic arrays of metallic NPs for two different reasons. First, SLRs can be associated with very high $Q$-factors and consequently also with considerable local-field enhancements. Second, the collective nature of SLRs makes them spatially dispersive, which can be utilized to realize broadband frequency conversion.

Collective SLRs result from radiative coupling between periodically arranged NPs. This coupling is strong near the Rayleigh anomaly wavelength, which for the first-order diffraction mode is given by [32]:

$$\lambda_{\pm 1} = P\,(n \mp \sin\,\theta)\,, \tag{3}$$

where $P$ is the array periodicity, $n$ is the refractive index of the surrounding material, and $\theta$ is the incidence angle in air, i.e. above the superstate material. Looking at equation (3), we see that the SLRs associated with diffraction orders $\pm 1$ occur at the same wavelength when $\theta = 0°$. When $\theta \neq 0°$, these two SLRs shift away from this wavelength, and from each other. This angle-dependence of SLRs provide simple means to tune the central wavelength of the resonance. We note that use of LSPRs does not provide similar tunability.

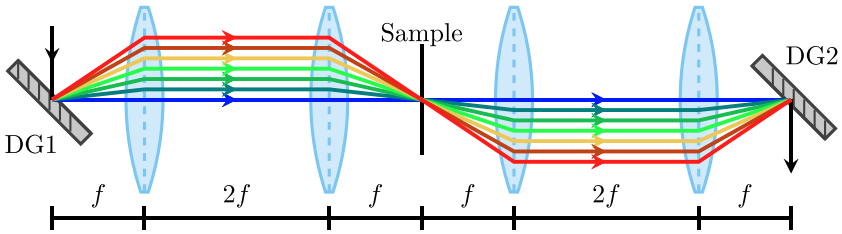


**Figure 1.** Proposed setup for broadband frequency conversion using high-$Q$ metasurfaces. The incident pulse is separated into its spectral components using the first diffraction grating (DG1). A 4$f$-correlator is then used to guide the spectral components into the metasurface, where the incidence angles $\theta$ of the spectral components depend on the frequency $\omega$. At the metasurface, the pump frequencies are up-converted with the process of sum-frequency generation. After the frequency conversion, the spectral components of the nonlinear signal are combined using a second 4$f$-correlator and a subsequent diffraction grating (DG2).

Despite the potential of utilizing high-$Q$ SLRs for enhancing light–matter interaction taking place in the metasurface, similar to all optical resonators their behavior is restricted by the time–bandwidth limit. An increase in the $Q$-factor of the resonator is necessarily associated with a reduction of the operation bandwidth. This limit seems to particularly restrict many nonlinear applications utilizing ultrashort laser pulses with pulse durations $\tau_p$ of 10–100 fs and linewidths $\Delta\lambda_L$ of 10–100 nm. Typical high-$Q$ SLRs have linewidths $\Delta\lambda_{SLR} \sim 1$ nm, suggesting their use with fs lasers to be inefficient. For example, when using a laser with $\tau_p \approx 200$ fs and $\Delta\lambda_L \approx 10$ nm, only ~10% of the laser power can be coupled into an SLR mode with a linewidth $\Delta\lambda_{SLR} = 1$ nm. To overcome this problem, we propose an experimental scheme that utilizes diffractive optical elements and the angle-dependent responses of SLRs (see figure 1).

The scheme for broadband frequency conversion using the setup shown in figure 1 consists of five steps and resembles closely a temporal focusing scheme [33, 34]. First, the incident laser pulse is split into its spectral components by a diffraction grating. The laser beam spot at the diffraction grating is then imaged using two lenses, acting as a 4$f$-correlator, onto the sample plane. Thus, the different spectral components of the input beam arrive to the sample at different angles of incidence $\theta$. With a properly selected diffraction grating and a set of lenses, the incidence angle of a given frequency component can be made to match with the resonance wavelength of the tilted SLR (see equation (3)). Therefore, it becomes possible to couple an incident broadband source more efficiently into a high-$Q$ metasurface and subsequently boost the broadband SFG response. Finally, using another pair of lenses acting as a 4$f$-correlator, the SFG signal component beams are imaged onto a second diffraction grating. With a proper selection of these components, the spectral components of the SFG signal are combined with the second diffraction grating completing the broadband conversion process.

## 2. Results and discussion

In this work, we used finite-difference time-domain (FDTD) method to simulate the optical response of a metasurface consisting of V-shaped aluminum NPs. In order to ensure homogeneous surroundings required for SLRs, the NPs were embedded inside homogeneous glass surroundings with refractive index $n = 1.51$. The NPs had arm length $L = 120$ nm, arm width $w = 70$ nm, and thickness $d = 30$ nm, resulting in LSPRs near 570 nm for $y$-polarized light (see figure 2). In order to have our metasurface exhibit $y$-polarized SLRs near 1000 nm, we set $p_x = 660$ nm. The other lattice constant was set to a slightly smaller value of $p_y = 400$ nm to increase the NP density without significant impact to the $y$-polarized SLRs. With these parameters and under illumination at normal incidence, the investigated metasurface exhibited an SLR at 1002 nm for $y$-polarized light. Here, linewidth of the SLRs was $\Delta\lambda_{SLR} \approx 2$ nm corresponding to $Q = 500$.

Next, we simulated the transmittance of the sample with the incidence angle $\theta$ varying from 0° to 9°. Again, we considered $y$-polarized light. By changing $\theta$, SLR peak was split into two peaks, which moved further from 1002 nm as $\theta$ increased (see figure 2 (b)). At $\theta = 9°$, SLRs occurred at 896 nm and 1100 nm. For the NP geometry considered in this work, the $Q$-factors and the local-field enhancement factors associated with the shorter-wavelength SLRs were found to be significantly lower than for those of the longer-wavelength SLRs. Therefore, in what follows, we chose to focus only on the longer-wavelength SLRs occurring between 1000–1100 nm.

In order to verify that the local fields are accordingly enhanced in the presence of high-$Q$ SLRs, we also present the simulated local field distributions (see figure 3). When using $y$-polarized incident light oscillating at the SLR peak wavelength, the light–matter interaction results in local-field hot spots near the corners of the NPs that point along the $y$-direction. Although the overall structure of the local-field

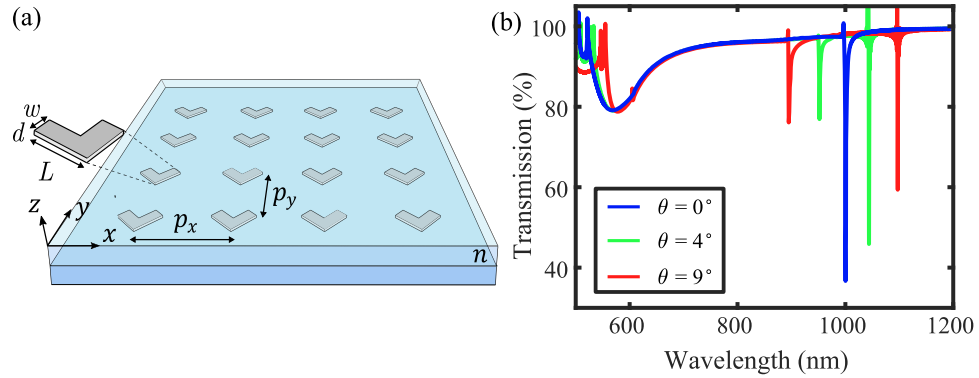


**Figure 2.** (a) The simulated metasurface consisting of V-shaped aluminum NPs arranged on rectangular lattice in homogeneous glass surroundings ($n = 1.51$). Here, the NP and lattice parameters are $L = 120$ nm, $w = 70$ nm, $d = 30$ nm, $p_x = 660$ nm, and $p_y = 400$ nm. (b) With these parameters and $y$-polarized incident light, the metasurface exhibits a broad LSPR near 570 nm and a much narrower SLR at 1002 nm. The simulated transmission spectra shows how the peak wavelengths of the splitted SLR near 1000 nm shift from the normal incidence resonance wavelength (blue line), when the incidence angle changes. With $\theta = 9°$ (red line) two SLRs form at 896 nm and 1100 nm. In this work, we chose to utilize only the SLRs occurring at longer wavelengths (>1000 nm), because their $Q$-factors are larger than those of the shorter-wavelength SLRs (<1000 nm).

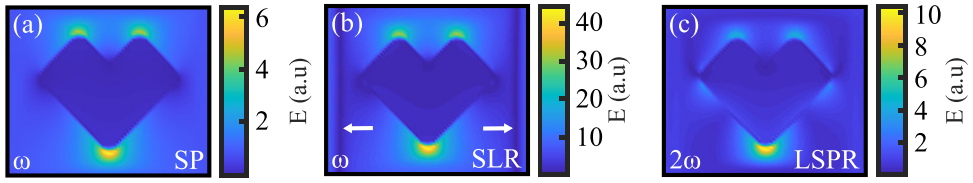


**Figure 3.** (a) Interaction with $y$-polarized light induces local-field hot spots on the edges of single particles (SP). (b) When nanoparticles are arranged in an array and the incident light is set to the SLR wavelength of 1002 nm, the local-field enhancement becomes dramatically larger than in the SP case. The collective nature of SLRs causes the field to drop symmetrically along the direction inter-particle coupling (white arrows). (c) At the second-harmonic wavelength of 501 nm, the local fields are enhanced due to the presence of a LSPR centered at 570 nm. In total, the mode overlap between $E(\omega, \mathbf{r})$ and $E(2\omega, \mathbf{r})$ result in enhanced SHG and SFG responses.

distribution associated with a single NP (figure 3(a)) is not markedly affected when the NPs are arranged periodically giving rise to the high-$Q$ SLR (figure 3(b)), the field amplitudes are. Their intensity dramatically increases, when we arrange particles into an array and couple light into the SLR mode (figure 3(b)). Clear local-field hot spots also form, when the wavelength of the incident light is close to the LSPR wavelength (figure 3(c)).

Next, we used the simulated field profiles (figure 3) to calculate mode-overlap integrals associated with the nonlinear scattering theory (see equations (1) and (2)). Here, we assumed that the nonlinear response of the plasmonic NPs is dominated by their surface response. Specifically, we only considered the susceptibility component perpendicular to the surface of the NP ($\chi^{(2)}_{\perp\perp\perp}$), and the respective field components [35]. Furthermore, the incident pump and the generated nonlinear signal fields were assumed to be polarized along the $y$-direction. First, we estimated how efficiently narrowband laser pulses ($\Delta\lambda_L \approx 1$ nm, FWHM) at different wavelengths between 1000–1100 nm can be converted to SHG wavelengths between 500–550 nm (see figure 4). Laser pulses at different wavelengths were guided on the metasurface at different incidence angles (0°–9°), resulting in enhanced SHG due to occurring SLRs. As expected by looking at equation (3), different incident wavelengths can be made resonant with the metasurface simply by changing the angle of incidence. When compared against the off-resonance situation (5 nm away from the SLR wavelength), the calculated SHG intensities were enhanced by factors in the range of 500 (8° angle of incidence) to 1800 (3° angle of incidence). The differences between SHG signals at different incident angles result from small differences in the pump and second-harmonic field distributions that affect the overall SHG signal levels due to changes in the mode-overlap calculations. Particularly, the estimated SHG signals were found to be very sensitive to the changes in the second-harmonic field.

Next, we consider the frequency conversion of a broadband laser pulse centered at a wavelength of 1050 nm having a bandwidth of $\Delta\lambda_L = 100$ nm (FWHM). First, we consider the situation where the entire pulse arrives at the metasurface at one incidence angle (see figure 5(a)). For simplicity, we assume that each spectral component of the broad laser pulse arrived at the metasurface simultaneously. Thus, the spectral

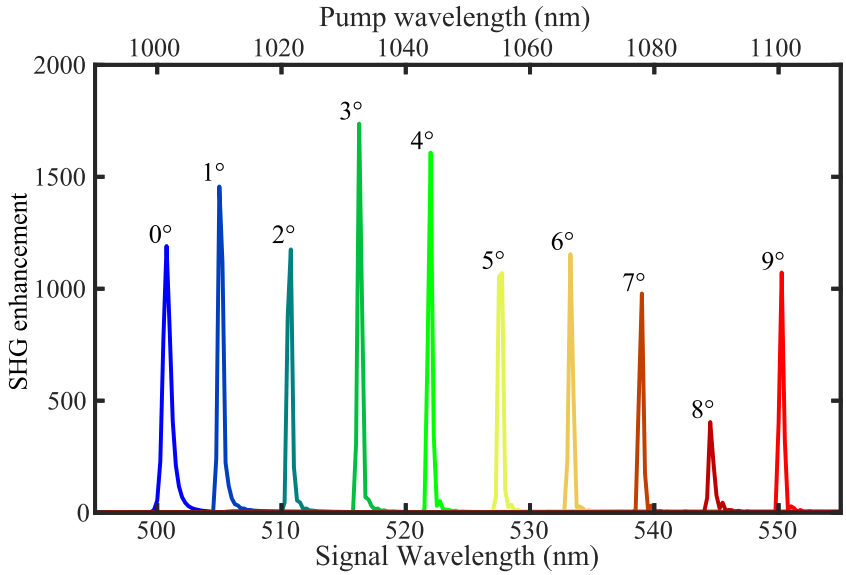


**Figure 4.** Tunable frequency conversion of narrowband laser pulses ($\Delta\lambda_L \approx 1$ nm) via angle-dependent SHG. The SHG signals are normalized to the non-resonant case (5 nm off the SLR wavelength).

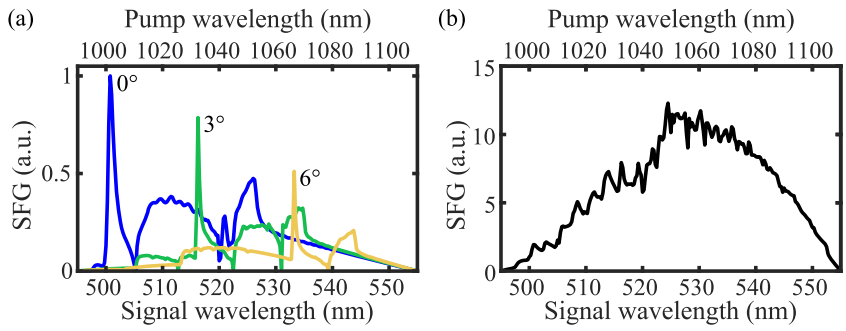


**Figure 5.** Frequency conversion of a broadband laser source ($\Delta\lambda_L = 100$ nm) via SFG in an SLR-supporting metasurface ($\Delta\lambda_{SLR} \approx 2$ nm corresponding to $Q = 500$). (a) SFG responses of studied metasurface without the proposed scheme (see figure 1). The laser pulse is incident on the metasurface at a single angle of incidence. Thus, the laser pulse arriving either at 0° (blue), 3° (green), or 6° (yellow) will be most efficiently converted only near the corresponding SLR wavelengths 1002 nm, 1032 nm, or 1067 nm, respectively. (b) The overall SFG response of the studied metasurface using the proposed scheme. Through the SLR-induced enhancement, all spectral components interact efficiently, resulting in a broadband frequency conversion with signal bandwidth $\Delta\lambda_{SFG} \approx 40$ nm (pump conversion bandwidth $\Delta\lambda \approx 75$ nm, 1020–1095 nm). All signals are normalized to the maximum SFG signal for the case where all spectral components arrive at $\theta = 0°$ (blue line).

components could interact with each other, resulting in numerous SFG signal wavelengths. However, efficient SFG occurs only when both pump fields are at the occurring SLR wavelength. Therefore, pumping at either 0°, 3°, or 6° results in strongest SFG emission at 500 nm, 516 nm, and 533 nm, respectively. At these strongest signal wavelengths, the SFG emission is enhanced by a factor of $\sim 1000$ when compared to the non-resonant situation. There are also weaker and broader emission peaks at longer wavelengths, for example, around 510 nm for illumination at $\theta = 0°$. These peaks arise from SFG processes where one of the pump fields is at the SLR wavelength while the other pump field is at an off-resonant wavelength.

Finally, we consider SFG emission for the situation with the proposed temporal focusing scheme (see figure 5(b)). We assume that the pulse is separated into 10 different spectral components each with a linewidth of 5 nm and constant and equal field amplitudes. Again, the spectral components arrive at the metasurface simultaneously, allowing them to interact with each other. This time, each component arrives at the metasurface at different incidence angles $\theta$ allowing each component to couple resonantly with an optimal SLR mode (see figure 2(b)). The occurring SLRs therefore enhanced the local fields at all the considered pump wavelengths, resulting in efficient SFG for numerous signal wavelengths. Remarkably, the numerous interactions combine to produce even stronger signal due to their cumulative nature. For example, the SFG process with the pump wavelengths $\lambda_1 = 1002$ nm and $\lambda_2 = 1100$ nm results in a nonlinear signal at the wavelength close to one gained with the process where $\lambda_1 = \lambda_2 = 1052$ nm, resulting

in stronger combined nonlinear emission near 525 nm. Due to the cumulative nature of the total SFG signal, the total SFG response is enhanced by an additional factor of 10, when compared to the calculated SFG spectra performed for individual angles of incidence. More importantly, the total SFG signal has a conversion bandwidth of $\Delta\lambda_{SFG} \approx 40$ nm (pump conversion bandwidth $\Delta\lambda \approx 75$ nm, 1020–1095 nm), indicating simultaneous resonance-enhanced and broadband frequency conversion of the initial laser pulse with $\Delta\lambda_L = 100$ nm. This conversion bandwidth $\Delta\lambda$ is almost 40 times broader than the linewidth $\Delta\lambda_{SLR} \approx 2$ nm associated with the normally incident SLR, suggesting a way to surpass the time–bandwidth limit by optimizing the way light is coupled into SLR-supporting metasurfaces.

We note that the simulated SFG emission spectrum would be narrower if we assumed Gaussian distribution for the incident broadband pulse. The spectral components at the pulse edges would have smaller amplitudes, reducing their nonlinear interaction strength and decreasing the SFG near 500 nm and 550 nm. Another factor that could considerably affect the SFG emission spectrum would be any possible chirp of the incident laser pulse. In that case, the different spectral components would not arrive at the metasurface simultaneously and could not interact efficiently with each other. The lack of interaction would limit the nonlinear processes to SHG, resulting in a nonlinear emission spectrum similar to one shown in figure 4. We note that even with these two limiting factors, the resulting overall nonlinear response would overcome the time–bandwidth limit associated with narrow resonances, such as SLRs.

The results above illustrate how our method results in broadband frequency conversion of light through the process of SFG. We believe that the method can be generalized to be applicable also for other nonlinear processes. For example, utilizing our approach for DFG or third-harmonic generation (THG), a broadband generation of THz or ultraviolet laser pulses could be achieved. We also note that the proposed method can be expected to be quite relevant when nonlinear responses of SLR-based metasurfaces with record-high $Q$-factors are investigated and utilized for frequency conversion applications [21].

As a whole, this numerical work proposes a novel methodology for broadband frequency conversion of light using metasurface-based high-$Q$ resonators ($Q \approx 500$). Because the time–bandwidth limit restricts the conversion bandwidth and the achievable efficiency of resonant nonlinear devices, the proposed methodology could provide new possibilities for metasurface-based broadband frequency conversion of light.

## 3. Conclusions

To conclude, we have demonstrated a method for a broadband frequency conversion using a metasurface supporting high-$Q$ SLRs ($Q \approx 500$). In our proposed setup design, different wavelength components are separated and guided on an SLR-supporting metasurface at different incident angles. Due to the spatial dispersion of SLRs, the scheme results in resonance-enhanced and broadband SFG response. Thus, our method is suitable for frequency conversion of both broadband laser pulses and of wavelength-tunable lasers with narrower spectral features. We have shown how the frequency conversion of an ultrashort laser pulse with a linewidth of 100 nm can be resonantly enhanced ($\sim$ 1000-fold) when comparing against non-resonant nonlinear response. Furthermore, a pump conversion bandwidth of $\Delta\lambda \approx 75$ nm is achieved, exceeding by almost a factor of 40 the linewidth (2 nm) of the SLR resonator. This result suggests a way to surpass the time–bandwidth limit associated with resonators by optimizing the way light is coupled into SLR-supporting metasurfaces. In addition to SFG and SHG, our method could be generalized for other frequency conversion processes, such as DFG and THG. Overall, our work opens new possibilities to perform broadband frequency conversion of light by utilizing high-$Q$ metasurface resonators.

## Acknowledgments

We acknowledge the support of the Academy of Finland (Grant No. 308596) and the Flagship of Photonics Research and Innovation (PREIN) funded by the Academy of Finland (Grant No. 320165). TS also acknowledges Jenny and Antti Wihuri Foundation for their PhD Grant.

## Data availability statement

The data that support the findings of this study are available upon reasonable request from the authors.

## Appendix A. Simulation methods

*Linear FDTD simulations.* The FDTD simulations were performed using lumerical FDTD solutions simulation software. We simulated the transmission spectra and local-field distribution for aluminum nanoparticles in homogeneous surroundings ($n = 1.51$). To investigate a periodic structure, we used periodic boundary conditions along the metasurface axes ($x$- and $y$-axes). The perfect-matching-layer (PML) conditions were used at the boundary along the initial propagation direction ($z$-axis). The PML profile was optimized for oblique-angle simulations. For simulations with $\theta \neq 0°$, we used the broadband fixed angle source technique (BFAST).

*Nonlinear scattering theory.* The nonlinear responses of our metasurface was evaluated using the presented nonlinear scattering theory and Lorentz reciprocity theorem [26, 27]. For simplicity, only the surface nonlinearities associated with metallic aluminum were considered. Furthermore, the component $\chi_{\perp\perp\perp}$ (all field components are perpendicular to the surface of the metal) was assumed to be the only non-zero susceptibility component describing the nonlinearities of the surfaces of the aluminum nanoparticles. We are not aware of studies reporting effective surface susceptibility tensor components for aluminum. Therefore, in this work the strength of the $\chi_{\perp\perp\perp}$ was set to unity, forcing also us to restrict to relative calculations. The calculations were performed with Matlab. There we used the local-field profiles simulated with FDTD as input values.

## ORCID iDs

Timo Stolt https://orcid.org/0000-0002-0047-8536
Mikko J Huttunen https://orcid.org/0000-0002-0208-4004

## References

[1] Maiman T H 1960 *Nature* **187** 493
[2] Boyd R W 2020 *Nonlinear Optics* 4th edn (New York: Academic) p 578
[3] Suchowski H, Oron D, Arie A and Silberberg Y 2008 *Phys. Rev.* A **78** 063821
[4] Suchowski H, Bruner B D, Ganany-Padowicz A, Juwiler I, Arie A and Silberberg Y 2011 *Appl. Phys.* B **105** 697
[5] Soukoulis C M and Wegener M 2011 *Nat. Photon.* **5** 523
[6] Klein M W, Enkrich C, Wegener M and Linden S 2006 *Science* **313** 502
[7] Alù A, Silveirinha M G, Salandrino A and Engheta N 2007 *Phys. Rev.* B **75** 155410
[8] Zhang S, Park Y-S, Li J, Lu X, Zhan W and Zhang X 2009 *Phys. Rev. Lett.* **102** 023901
[9] Genevet P, Capasso F, Aieta F, Khorasaninejad M and Devlin R 2017 *Optica* **4** 139
[10] Kauranen M and Zayats A V 2012 *Nat. Photon.* **6** 737
[11] Maier S A 2007 *Plasmonics: Fundamentals and Applications* (Berlin: Springer)
[12] Lapine M, Shadrivov I V and Kivshar Y S 2014 *Rev. Mod. Phys.* **86** 1093
[13] Butet J, Brevet P-F and Martin O J F 2015 *ACS Nano* **9** 10545
[14] Li G, Zhang S and Zentgraf T 2017 *Nat. Rev. Mater.* **2** 17010
[15] Li G *et al* 2017 *Nano Lett.* **17** 7974
[16] Rahimi E and Gordon R 2018 *Adv. Opt. Mater.* **6** 1
[17] Huttunen M J, Czaplicki R and Kauranen M 2019 *J. Nonlinear Opt. Phys. Mater.* **28** 1950001
[18] Wu T *et al* 2019 *Adv. Opt. Mater.* **7** 1900905
[19] Kravets V G, Kabashin A V, Barnes W L and Grigorenko A N 2018 *Chem. Rev.* **118** 5912
[20] Utyushev A D, Zakomirnyi V I and Rasskazov I L 2021 *Rev. Phys.* **6** 100051
[21] Bin-Alam M S *et al* 2021 *Nat. Commun.* **12** 974
[22] Michaeli L, Keren-Zur S, Avayu O, Suchowski H and Ellenbogen T 2017 *Phys. Rev. Lett.* **118** 243904
[23] Hooper D C, Kuppe C, Wang D, Wang W, Guan J, Odom T W and Valev V K 2018 *Nano Lett.* **19** 165
[24] Huttunen M J, Reshef O, Stolt T, Dolgaleva K, Boyd R W and Kauranen M 2019 *J. Opt. Soc. Am.* B **36** E30
[25] Fan S, Suh W and Joannopoulos J D 2003 *J. Opt. Soc. Am.* A **20** 569
[26] Roke S, Bonn M and Petukhov A V 2004 *Phys. Rev.* B **70** 115106
[27] O'Brien K, Suchowski H, Rho J, Salandrino A, Kante B, Yin X and Zhang X 2015 *Nat. Mater.* **14** 379
[28] Wang F, Martinson A B F and Harutyunyan H 2017 *ACS Photonics* **4** 1188
[29] Wu T, Luo Y, Maier S A and Wei L 2019 *Phys. Rev. Appl.* **11** 014049
[30] Noor A, Damodaran A R, Lee I-H, Maier S A, Oh S-H and Ciracì C 2020 *ACS Photonics* **7** 3333
[31] Huttunen M J, Dolgaleva K, Törmä P and Boyd R W 2016 *Opt. Express* **24** 28279
[32] Khlopin D *et al* 2017 *J. Opt. Soc. Am.* B **34** 691
[33] Oron D, Tal E and Silberberg Y 2005 *Opt. Express* **13** 1468
[34] Block E, Greco M, Vitek D, Masihzadeh O, Ammar D A, Kahook M Y, Mandava N, Durfee C and Squier J 2013 *Biomed. Opt. Express* **4** 831
[35] Wang F X, Rodríguez F J, Albers W M, Ahorinta R, Sipe J E and Kauranen M 2009 *Phys. Rev.* B **80** 4